Acoustic Stack for Combined Intravascular Ultrasound and Photoacoustic Imaging

Antonio López-Marín, *Member, IEEE*, Verya Daeichin, *Member, IEEE*, Andres Hunt, Geert Springeling, Robert Beurskens, Antonius F. W. van der Steen, *Fellow, IEEE*, and Gijs van Soest

***Abstract*—Multimodal intravascular ultrasound and photoacoustic (IVUS/PA) imaging is a promising diagnostic tool for cardiovascular diseases like atherosclerosis. IVUS/PA catheters typically require two independent transducers due to different frequency requirements, potentially increasing the catheter size. To facilitate multimodal imaging within conventional catheter dimensions, we designed, fabricated, and characterized a dual-transducer acoustic stack where a low-frequency (LF) PA receiver sits as a matching layer for the high-frequency (HF) US transducer. While the HF transducer operates around 50 MHz, the LF receiver targets frequencies below 15 MHz to capture most of the PA energy from atherosclerotic plaque lipids. Simulation results reveal that this configuration could increase the sensitivity of the HF transducer by 3.54 dB while maintaining bandwidth. Phantom experiments with fabricated stacks showed improved performance for the US transducer, validating the enhanced sensitivity and bandwidth. Following improvements in stack fabrication, the proposed acoustic stack is a viable design that can significantly enhance diagnostic accuracy for atherosclerosis, providing high-resolution, multifrequency imaging within a compact catheter form factor.**

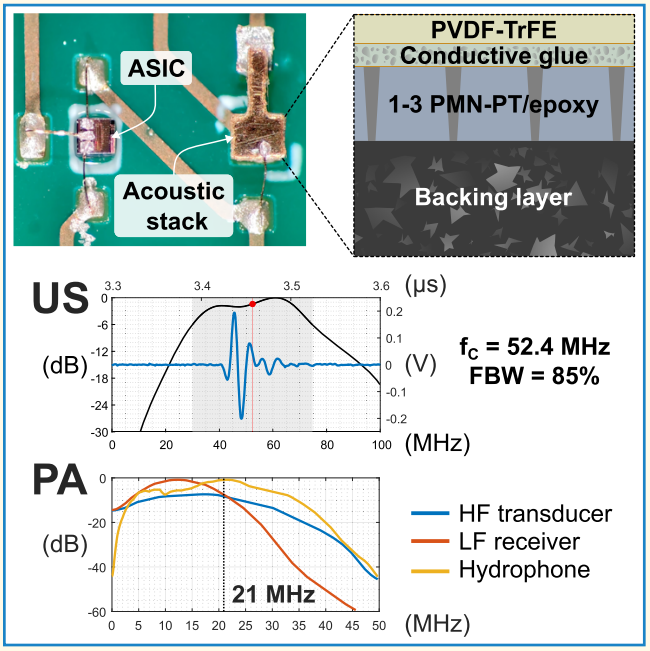

***Index Terms*—Catheters, manufacturing, numerical simulation, photoacoustic (PA) imaging, transducers, ultrasound.**

Received 26 June 2024; accepted 17 September 2024. Date of publication 23 September 2024; date of current version 27 January 2025. This work was supported in part by the Medical Delta Scientific Program, The Netherlands, under Project Novel Instruments for Minimally Invasive Techniques (NIMIT). *(Corresponding author: Antonio López-Marín.)*

Antonio López-Marín and Robert Beurskens are with the Department of Cardiology, Thorax Center, Cardiovascular Institute, Erasmus MC University Medical Center, 3015 GD Rotterdam, The Netherlands (e-mail: a.lopezmarin@erasmusmc.nl).

Verya Daeichin is with Kaminari Medical B.V., Erasmus MC University Medical Center, 3015 GD Rotterdam, The Netherlands.

Andres Hunt is with the Department of Precision and Microsystems Engineering, Delft University of Technology, 2628 CD Delft, The Netherlands.

Geert Springeling is with the Department of Experimental Medical Instrumentation, Erasmus MC University Medical Center, 3015 GD Rotterdam, The Netherlands.

Antonius F. W. van der Steen is with the Department of Cardiology, Thorax Center, Cardiovascular Institute, Erasmus MC University Medical Center, 3015 GD Rotterdam, The Netherlands, and also with the Department of Imaging Physics, Delft University of Technology, 2628 CJ Delft, The Netherlands.

Gijs van Soest is with the Department of Cardiology, Thorax Center, Cardiovascular Institute, Erasmus MC University Medical Center, 3015 GD Rotterdam, The Netherlands, also with the Department of Precision and Microsystems Engineering, Delft University of Technology, 2628 CD Delft, The Netherlands, and also with the Wellman Center for Photomedicine, Harvard Medical School and Massachusetts General Hospital, Boston, MA 02114 USA (e-mail: g.vansoest@erasmusmc.nl).

Digital Object Identifier 10.1109/TUFFC.2024.3465837

I. Introduction

CARDIOVASCULAR diseases, particularly coronary atherosclerosis, are the leading cause of mortality worldwide [1]. Atherosclerosis now impacts younger and more diverse populations worldwide, with studies highlighting the impact of inflammation, genetics, and lifestyle factors such as sleep, physical activity, and stress [2]. Intravascular ultrasound (IVUS) is an established technology used for image guidance during percutaneous coronary intervention (PCI), a procedure used to diagnose and treat coronary artery disease. The combination of IVUS and intravascular photoacoustic (IVPA) imaging is a hybrid modality that has emerged as a promising alternative for detecting and characterizing atherosclerotic plaques [3]. Photoacoustic (PA) imaging uses pulsed light to excite optically absorbing materials to generate an ultrasonic response. While IVUS provides anatomical volumetric imagery of the artery, IVPA provides chemical-specific optical information about the components inside the plaque, which is accessible by a judicious choice of near-infrared excitation wavelengths. At these wavelengths, the absorption from plaque components is greater than from surrounding tissue and blood, governed by water, thus providing sufficient optical contrast [4]. Previous research demonstrated that the PA signal

Highlights

- **A vertically stacked dual-transducer configuration enables multimodal IVUS/PA imaging while minimizing probe tip size, which is essential for catheter deliverability.**
- **Simulations and experiments demonstrate an intravascular-compatible configuration where PVDF-TrFE can function both as a LF receiver and a matching layer, enhancing the performance of the HF transducer.**
- **This acoustic stack design can accelerate clinical translation of IVPA imaging and potentially improve atherosclerosis diagnosis by providing high-resolution, multifrequency imaging in a compact form.**

frequency inversely correlates with the size of absorbing structures [5], and the bulk of the PA energy content from human coronary plaques lies between frequencies of 2 and 15 MHz [6].

Several combined intravascular ultrasound and photoacoustic (IVUS/PA) catheter concepts have been presented previously, employing various methods to capture PA signals. The most common approach is to use one piezoelectric transducer for IVUS and IVPA imaging [7], [8], [9], [10], [11], [12], [13], [14], [15], a simple solution that only necessitates aligning the optical beam from a fiber to the ultrasound field of view. More complex designs used a ring transducer that ensured collinear acquisition of US and PA signals by fitting a fiber through the transducer's central hole [16], [17], [18]. Alternative IVPA catheters rely on an optical ultrasound detection approach using optical resonators like micro-ring resonators (MRRs) [19], [20], or Fabry-Perot cavities [21], [22]. However, these solutions add to the complexity of the catheter fabrication compared to piezoelectric transducers solutions.

IVUS piezoelectric transducers typically have center frequencies between 40 and 60 MHz, favoring high frequency for increased pulse-echo resolution but resulting in suboptimal sensitivity to the lower frequencies in the PA signal. A PA receiver covering a wide frequency range of 2–15 MHz would provide high PA sensitivity in atherosclerotic plaque imaging. Multitransducer configurations have been proposed to enhance resolution and viewing depth [23], as well as sensitivity to the PA signal, by adding a second transducer with a center frequency of 23 MHz [24]. We previously demonstrated a receiver based on a PVDF sensor and a miniature low-noise amplifier to target PA detection in the 2–15 MHz frequency range [25]. A dual-transducer IVUS/PA catheter using this receiver along a high-frequency (HF) transducer would improve IVPA sensitivity while maintaining IVUS resolution. Configurations featuring multiple transducers have also been implemented in IVUS catheters [26], [27], [28], [29]. However, space comes at a premium in coronary catheters, which have a practical upper limit for the outer diameter of <1 mm, while the rigid length of the tip should be minimized to maintain the deliverability of the catheter. Including an extra transducer can increase the catheter tip size beyond these practical limits.

Here, we propose a vertically stacked configuration that accommodates a HF transducer for IVUS imaging and a low-frequency (LF) transducer working as a PA receiver. The use of a piezoelectric polymer for the LF transducer renders it transparent to the signals being transmitted from and received by the HF transducer, which has a higher acoustic impedance. Thus, the LF transducer also acts as a matching layer for the IVUS element in this configuration. Designs featuring stacked transducers have already been proposed for simultaneous therapy and monitoring with ultrasound contrast agents [30], [31], [32]. Previous designs have also demonstrated the viability of fabricating miniaturized stacks with matching layers in the order of 10 μm [33], [34]. In this work, we developed a compact dual-transducer acoustic stack to deliver co-registered PA and US images, intended for use in an intravascular catheter. The acoustic performance of the hybrid stack was simulated to identify optimal manufacturing parameters. Following fabrication, the stack samples were characterized through phantom experiments. These initial results indicate that the proposed design holds promise for developing an improved diagnostic catheter for IVUS/PA imaging applications.

II. Materials and Methods

A. Stack Design

The main components of the dual-transducer stack are the HF transducer and the LF receiver. The HF element is a 1–3 PMN-PT/epoxy piezocomposite (CTS Corporation, Lisle, IL, USA) with a mechanical resonance frequency f_R around 50 MHz, 60% crystal volume fraction, coupling coefficient $k_t > 0.7$, and 25-μm thickness. The element lies on a 300-μm conductive epoxy-backing layer with a top electrode, and it has an active area of 533×432 μm. The LF receiver element consists of poly(vinylidene fluoride-trifluoroethylene) (PVDF-TrFE). As previously demonstrated [25], this PA receiver uses an external application-specific integrated circuit (ASIC) to match the impedance between the polymer and the connecting cable and amplify the captured PA signals in the 2–15 MHz range. Within this frequency range, the receiver is sensitive enough to detect pressures down to 30 Pa and can amplify incoming PA signals up to 18.4 dB, with an output noise level of 259 μV_{RMS} across its entire bandwidth.

Fig. 1 shows the initial acoustic stack design, including the concept for integration into a future imaging catheter. At the top of the stack, a PVDF-TrFE layer acts as a transducer and a matching layer for the underlying piezocomposite transducer. A conductive glue layer sits between these transducers to provide mechanical and electrical bonding as a common ground electrode. We chose silver-loaded epoxy for this layer due to its availability and potential manufacturability. The stack configuration allows the piezocomposite to be connected

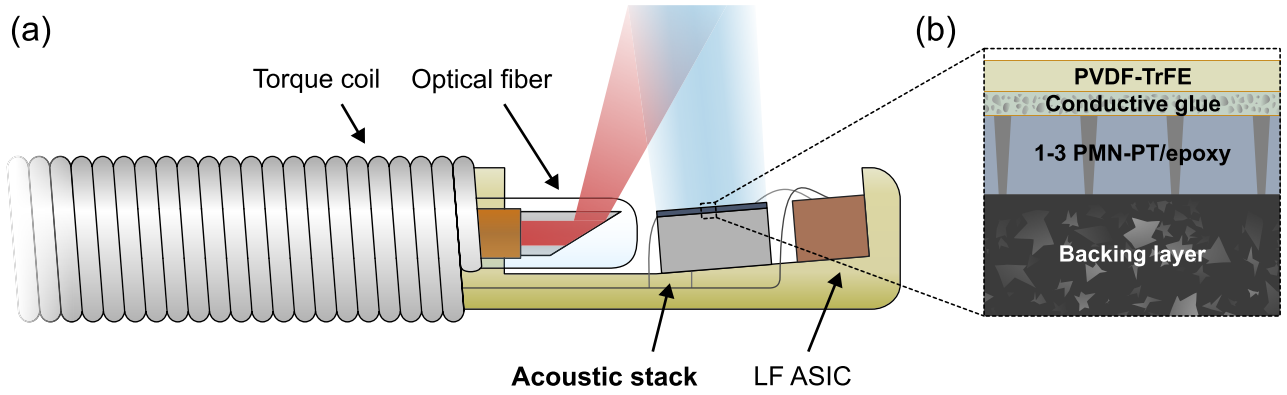

Fig. 1. (a) Diagram of the proposed acoustic stack sitting in the tip of a combined IVUS/PA catheter. (b) Schematic of the top section of the acoustic stack and the interface between its layers. Catheter and stack dimensions are not depicted to scale.

via the conductive backing while enabling access to the PVDF-TrFE transducer through an electrode on the top of the stack.

Model simulations can be performed to evaluate the design, and they will require determining specific layer parameters that are unknown beforehand. A 1-D model is helpful to run a large number of iterations. For this case, the 1–3 piezocomposite should be replaced with a single-phase material whose effective parameters can be determined using the following equations [35]:

$$\bar{c}_{33}^{E} = v_c\left[c_{33}^{E} - \frac{2(1-v_c)\left(c_{13}^{E}-c_{12}\right)^2}{v_c(c_{11}+c_{12})+(1-v_c)\left(c_{11}^{E}+c_{12}^{E}\right)}\right] + (1-v_c)c_{11} \tag{1}$$

$$\bar{e}_{33} = v_c\left[e_{33} - \frac{2(1-v_c)e_{31}\left(c_{13}^{E}-c_{12}\right)}{v_c(c_{11}+c_{12})+(1-v_c)\left(c_{11}^{E}+c_{12}^{E}\right)}\right] \tag{2}$$

$$\bar{\varepsilon}_{33}^{S} = v_c\left[\varepsilon_{33}^{S} - \frac{2(1-v_c)(e_{31})^2}{v_c(c_{11}+c_{12})+(1-v_c)\left(c_{11}^{E}+c_{12}^{E}\right)}\right] + (1-v_c)\varepsilon_{11} \tag{3}$$

$$\bar{c}_{33}^{D} = \bar{c}_{33}^{E} + \left(\bar{e}_{33}\right)^2 \Big/ \bar{\varepsilon}_{33}^{S} \tag{4}$$

where v_c is the crystal volume fraction, c_{11}^{E}, c_{12}^{E}, c_{13}^{E} and c_{33}^{E} are elastic constants of the crystal, c_{11} and c_{12} are elastic constants of the polymer; e_{31} and e_{33} are the piezoelectric constants of the crystal, ε_{33}^{S} and ε_{11} are the dielectric constants for crystal and polymer, respectively, and $\bar{c}_{33}^{E}$, $\bar{c}_{33}^{D}$, $\bar{e}_{33}$, and $\bar{\varepsilon}_{33}^{S}$ are the elastic, piezoelectric, and dielectric constants for the piezocomposite, respectively; and

$$\bar{\rho} = v_c \cdot \rho_c + (1-v_c)\rho_p \tag{5}$$

$$\bar{k}_t = \bar{e}_{33} \Big/ \sqrt{\bar{c}_{33}^{D} \cdot \bar{\varepsilon}_{33}^{S}} \tag{6}$$

$$\bar{Z} = \sqrt{\bar{c}_{33}^{D} \cdot \bar{\rho}} \tag{7}$$

$$\bar{c_L} = \sqrt{\bar{c}_{33}^{D} / \bar{\rho}} \tag{8}$$

where ρ_c and ρ_p are the density values for crystal and polymer, and $\bar{\rho}$, $\bar{k}_t$, $\bar{Z}$ and $\bar{c_L}$ are the effective density, electromechanical coupling coefficient, acoustic impedance, and longitudinal velocity for the piezocomposite, respectively.

The thickness of the matching layers was calculated as the quarter wavelength ($\lambda/4$) thickness based on the piezocomposite working frequency of 50 MHz. The ideal acoustic impedance values for the two layers can be determined using the following equations [36]:

$$Z_1 = \sqrt[7]{\bar{Z}^4 \cdot Z_0^3}, \quad Z_2 = \sqrt[7]{\bar{Z} \cdot Z_0^6} \tag{9}$$

where Z_0 is the acoustic impedance value of the medium. While the impedance of PVDF-TrFE is known and different from Z_2, a value Z_1 for the silver-epoxy composite can be controlled by choosing the optimal silver volume fraction using the following equations [37]:

$$\bar{K} = K_p + v_s \frac{\left(3\bar{K}+4\bar{G}\right)\left(K_s-K_p\right)}{3\bar{K}+4\bar{G}+3\left(K_s-K_p\right)} \tag{10}$$

$$\bar{G} = G_p + v_s \frac{5\bar{G}\left(3\bar{K}+4\bar{G}\right)\left(G_s-G_p\right)}{\bar{G}\left(15\bar{K}+20\bar{G}\right)+6\left(\bar{K}+2\bar{G}\right)\left(G_s-G_p\right)} \tag{11}$$

$$\bar{\rho} = v_s \cdot \rho_s + (1-v_s) \cdot \rho_p \tag{12}$$

$$\bar{c_L} = \sqrt{\left(\bar{K}+4\bar{G}/3\right)/\bar{\rho}} \tag{13}$$

$$\bar{Z} = \bar{c_L} \cdot \bar{\rho} \tag{14}$$

where $\bar{K}$, K_p, and K_s are the bulk moduli of composite, polymer matrix, and scatterer, respectively; $\bar{G}$, G_p and G_s are the shear moduli of the composite, polymer matrix, and scatterer, respectively; v_s is the silver volume fraction, ρ_s, ρ_p are the density values of silver and polymer; and $\bar{\rho}$, $\bar{c_L}$, and $\bar{Z}$ and are the composite's density, acoustic impedance, and longitudinal velocity, respectively. Fig. 2 shows the values calculated for $\bar{c_L}$ and $\bar{Z}$ based on the volume fraction of silver. The parameters of PMN-28%PT, epoxy, and silver used in the previous calculations are presented in Table I.

Based on initial parameters for the acoustic stack, a 1-D model was implemented in MATLAB (2023b, MathWorks, Natick, MA, USA) based on the Krimholtz, Leedom, and Matthaei (KLM) equivalent circuit [38] to assess the pulse-echo performance of the design. An initial bare stack model without matching layers was used as a reference for comparison. We conducted a parameterization study with three variables within a ±50% range around the initial parameters: thickness and silver volume fraction of the conductive glue layer and thickness of the PVDF-TrFE layer. We also

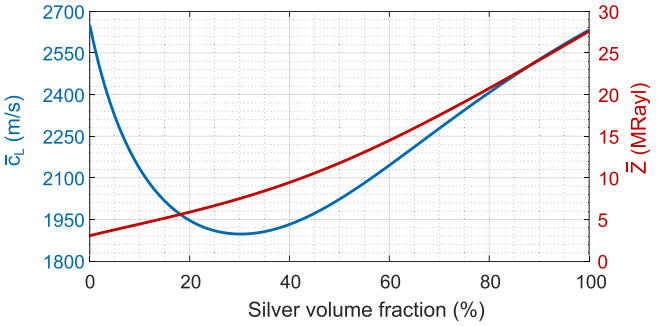

Fig. 2. Longitudinal velocity ($\bar{c}_L$, blue) and acoustic impedance ($\bar{Z}$, red) of a silver-loaded epoxy composite.

TABLE I
COMPOSITE MATERIAL PROPERTIES

Material	Properties	
PMN-28%PT	ρ_c = 8100 kg/m^3	$\varepsilon^S_{11} = 1368 \cdot \varepsilon_0$
	$\varepsilon^S_{33} = 895 \cdot \varepsilon_0$	$c^E_{11} = 11.58 \cdot 10^{10}$ N/m^2
	$c^E_{12} = 10.23 \cdot 10^{10}$ N/m^2	$c^E_{13} = 9.31 \cdot 10^{10}$ N/m^2
	$c^E_{33} = 10.71 \cdot 10^{10}$ N/m^2	$c^E_{44} = 6.44 \cdot 10^{10}$ N/m^2
	$c^E_{66} = 6.01 \cdot 10^{10}$ N/m^2	e_{31} = -13.12 C/m^2
	e_{33} = 21.72 C/m^2	e_{15} = 8.69 C/m^2
Epoxy	ρ_p = 1150 kg/m^3	$\varepsilon_{11} = 3.8 \cdot \varepsilon_0$
	$c_{11} = 0.81 \cdot 10^{10}$ N/m^2	$c_{12} = 0.46 \cdot 10^{10}$ N/m^2
	$K_p = 5.76 \cdot 10^9$ Pa	$G_p = 1.74 \cdot 10^9$ Pa
Silver	ρ_s = 10490 kg/m^3	
	$K_s = 110 \cdot 10^9$ Pa	$G_s = 30 \cdot 10^9$ Pa

ρ: density, c: stiffness constant, e: piezoelectric coupling constant, ε: dielectric constant, K: bulk modulus, G: shear modulus

simulated 1000 transducer configurations in a Monte Carlo approach, each with randomly chosen combinations of the three parameters. The results allow us to assess the net sensitivity to variations in these parameters, all of which have a finite tolerance when manufacturing the final stack. For each variable combination, the result was evaluated based on key performance indicators (KPIs) from the echo frequency response: peak value A_{PEAK}, center frequency f_C, and −6 dB bandwidth FBW, calculated as follows:

$$A_{PEAK} = \max|\text{Echo}(f)| \tag{15}$$

$$f_C = \frac{f_L + f_U}{2} \tag{16}$$

$$\text{FBW} = \frac{f_U - f_L}{f_C} \tag{17}$$

where f_U and f_L are the upper and lower frequencies for which the frequency response falls to half from the peak value. An extra indicator was defined based on the other three KPIs to find the optimal stack, a figure of merit (FOM) that can be calculated as follows:

$$\text{FOM} = \frac{A_{PEAK}}{A_{PEAK0}} \cdot \text{FBW} \cdot \frac{f_{C0}}{\alpha f_{C0} + |f_C - f_{C0}|} \tag{18}$$

where A_{PEAK0} and f_{C0} are the peak value and the center frequency of the bare stack, respectively, and α is a factor that modulates how much the FOM penalizes deviations of f_C from f_{C0}: smaller α increases the sensitivity to deviations, while larger α reduces it. The maximum value for the FOM reveals a combination of variables that provide an optimized acoustic stack, favoring high sensitivity and FBW while keeping f_C close to f_{C0}. FOM values can help select an optimal design, but they do not accurately reflect its actual performance. The optimized stack was used as a starting point for a Monte Carlo tolerance analysis to determine the effect of manufacturing variability on the different KPIs.

An additional model was designed in OnScale Lab (Ansys Inc., Canonsburg, PA, USA) to more accurately evaluate the effect of the glue thickness, representing the piezocomposite as a more geometrically precise structure, close to real-world conditions. The conductive backing layer material was selected from one of the predefined options available in OnScale Lab. We conducted a parametric simulation study varying the glue thickness and analyzing the same KPIs defined before to choose the suitable value for the stack fabrication. The initial parameters for the KLM and OnScale Lab models are presented in Table II.

B. Stack Fabrication

Using the results of the parameterization study and tolerance analysis, we selected commercially available components for the fabrication of the matching layers. We chose Loctite Ablestik 56C CAT9 (Henkel, Düsseldorf, Germany) as conductive glue, with an estimated silver volume concentration of 21.5% and 6.07 MRayl acoustic impedance using (10)–(14) and manufacturer's specifications. The PVDF-TrFE material (PolyK, Philipsburg, PA, USA) was also acquired off-the-shelf. It is uni-axially polarized, with 100-nm gold electrodes on both sides, and is available in different thicknesses and polymer compositions. The only variable left that can affect ultrasound performance is the thickness of the conductive glue.

The building process of the stack was performed from top to bottom. Fig. 3(a) shows a diagram of the process. First, the PVDF-TrFE transducer material was put in place on top of a microscope slide. We used a custom-built device to manually apply the first matching layer of silver-epoxy glue with a controlled thickness in the stack. After putting enough glue on top of the sample, the device allows to evenly distribute it to the desired thickness with micrometer accuracy. The slide was then removed from the device, a few bare transducers were manually placed upside down on the glue, and it was later oven-heated at 50 °C for 2 h to cure the glue. The matching layers' material around the stacks was cut using a femtosecond (LS-Lab, Lasea S.A., Pessac, France) or a nanosecond (WS-Starter, Optec S.A., Frameries, Belgium) pulsed laser cutter to separate them from the slide. Fig. 3(b) shows a picture of the stack after laser cutting, where only backing and glue layers are clearly visible.

C. Stack Characterization

To test each stack, we designed a printed circuit board (PCB) [see Fig. 4(a)] that can hold and interconnect stack and ASIC and provide breakout pins for all traces for external connectivity. All the stack layers were connected to the traces using conductive epoxy and gold wiring, except for a thick

TABLE II
STACK MODEL INITIAL LAYER PROPERTIES

Layer	Material	Properties				
		ρ (kg/m^3)	c_L (m/s)	Z (MRayl)	t (μm)	Additional
Conductive backing	Tungsten-loaded epoxy	4800	1800	8.6	300	v_T = 20%, α_B =10 dB/MHz/cm
1-3 piezocomposite	PMN-28%PT / epoxy	5320	4142	22.03	25	v_C = 60%, w_K = 2.5 μm
1st matching layer	Silver-loaded epoxy	3672	1902	6.94	9.4	v_S = 27%, α_B = 7 dB/MHz/cm
2nd matching layer	PVDF-TrFE	1800	2350	4.23	11.8	α_B = 3 dB/MHz/cm
Medium	Water	1000	1500	1.50		α_B = 0.02 dB/MHz/cm

ρ: density, c_L: longitudinal velocity, Z: acoustic impedance, v_T: tungsten volume fraction, v_C: single crystal volume fraction, v_S: silver volume fraction, t: thickness, w_K: kerf width, α_B: bulk attenuation

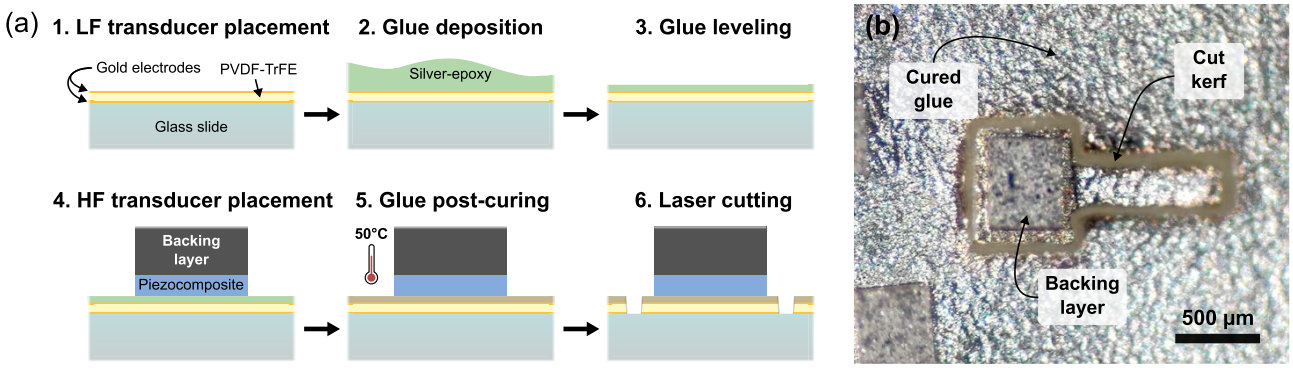

Fig. 3. (a) Schematic of the fabrication steps for the acoustic stack. Layer dimensions are not depicted to scale. (b) Magnified image of the bottom of the stack after the last fabrication step (laser cutting). LF: low frequency, HF: high frequency.

metallic wire to connect the common ground. Fig. 4(b) illustrates the interface configuration, where the HF transducer can be connected directly to an external device. The LF transducer can be read out with a single cable via the ASIC, with a splitter required to separate the PA signal from ASIC power, which is provided on the same cable. This configuration is further detailed in our previous study [25].

The acoustic stack performance for ultrasound imaging using the HF transducer was tested using a pulse-echo system illustrated in Fig. 5(a). The piezocomposite was driven using a pulser-receiver (PureView Hb3, JSR Ultrasonics, Pittsford, NY, USA) connected through a 20-dB attenuator (HAT-20+, Mini Circuits, Brooklyn, NY, USA). The pulser-receiver amplified the echo signal by 30 dB, to be then recorded using a 14-bit 400-MSa/s acquisition card (PX14400A, Signatec, Lockport, IL, USA) installed in a personal computer (PC). The PCB was attached to an adaptor held by a three-axis positioning system (MP63-3, Steinmeyer, Albstadt, Germany) controlled by the PC. The PCB side with the stack was submerged in a tank with demineralized water. Two different targets were used to evaluate the HF transducer performance: a silver-coated mirror (PF10-03-P01, Thorlabs, Newton, NJ, USA) for time and frequency response and a 15-μm Pt-Ir wire (Degussa GmbH, Munich, Germany) for spatial resolution. The targets were placed at the natural focus of the HF transducer, around 2.4 mm away from the front surface of the stack. The raw data acquisition and motor control program was developed in C++. Further signal processing was performed in MATLAB.

The stack performance as a broadband receiver was evaluated with a PA experiment where the HF and LF transducers receive a PA signal generated by an absorber at a distance.

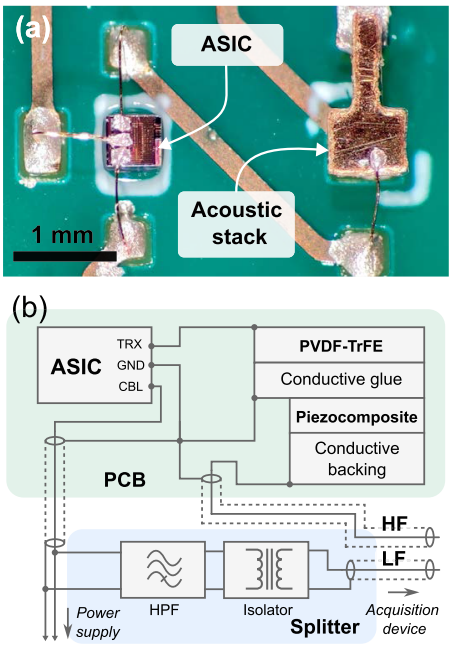

Fig. 4. (a) Magnified image of a populated PCB with acoustic stack and ASIC. (b) Schematic showing the connections between PCB elements and with external devices. HPF: high-pass filter, HF: high frequency, LF: low frequency.

Fig. 5(b) shows a diagram of the setup. Black duct tape (74613, Tesa, Norderstedt, Germany) was placed on the bottom of a water tank as the PA absorber. Two slit fiber bundles were air-coupled to a tunable diode-pumped OPO laser (Spitlight EVO-OPO, InnoLas GmbH, Krailling, Germany) that

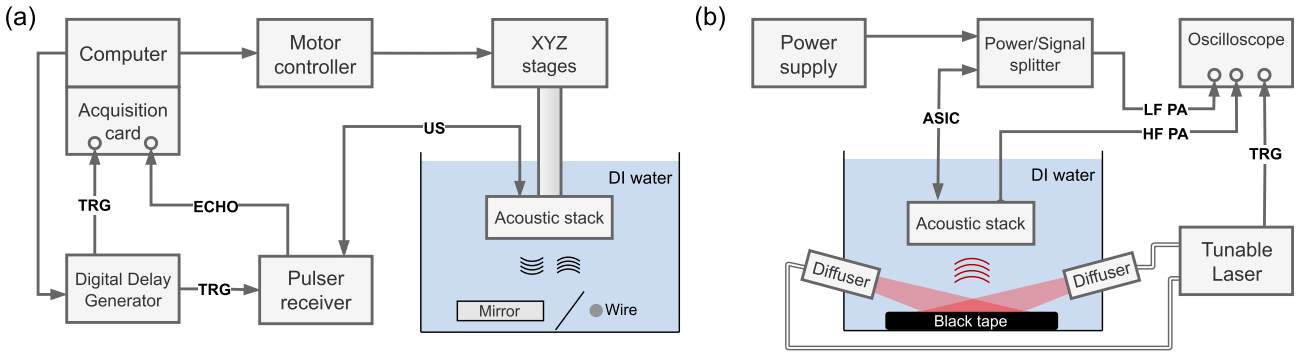

Fig. 5. (a) Pulse-echo stack characterization setup. (b) PA stack characterization setup. Electrical and optical connections and indicated with single and double wires, respectively. DI: Deionized (water), TRG: trigger, US: ultrasound, LF PA: Photoacoustic response from low-frequency transducer, HF PA: Photoacoustic response from high-frequency transducer.

TABLE III
STACK MODEL PARAMETERS

Model	t_{ML1}	t_{ML2}	v_S
1-D (Initial)	9.4 µm	11.8 µm	27%
1-D (Optimized)	8.3 µm	9.1 µm	34%
3-D	7.0 µm	9.0 µm	21.5%

t: thickness, M1: first matching layer, M2: second matching layer, v_S: silver volume fraction.

illuminated the absorber with 100-Hz repetition rate, 5-ns laser pulses with 950-nm wavelength. The PA signal originating from the tape was first recorded using a 0.2 mm PVDF needle hydrophone (NH0200, Precision Acoustics, Dorchester, U.K.) at a distance of 15 mm. The same experiment was performed with the PCB sample at the same position. All the signals were recorded with an oscilloscope (DSO5034A, Agilent, Santa Clara, CA, USA) and postprocessed in MATLAB.

III. RESULTS

A. Stack Simulations

The parameters for the matching layers used in the different models are presented in Table III. A bare stack model was designed without the matching layers on top. We calculated the pulse-echo response by simulation using the KLM model of the bare stack [see Fig. 6(a)] and the acoustic stack with initial values [see Fig. 6(b)]. This initial stack echo amplitude almost doubles that of the bare stack. The echo response of the optimized stack with maximum FOM in Fig. 6(c) reveals that it is possible to increase sensitivity by 8.46 dB further while keeping the FBW at a value similar to the bare stack. Fig. 6(d) illustrates the comparison of the different stack frequency responses.

The pulse-echo acoustic performance, simulated using the KLM model with randomly varying thicknesses of both matching layers and the silver volume fraction in the first matching layer around their optimal values, is presented in Fig. 6(e). The Pearson's correlation coefficient (r) for each graph represents the dependency between each stack parameter and KPI. There is a strong correlation between the thickness of the matching layers and the sensitivity, bandwidth, and center frequency. Thinner matching layers produce lower bandwidth and higher center frequency but greater sensitivity. In comparison, the variance in the volume fraction of silver in the composite glue does not affect the stack's performance as strongly. Based on the KLM model results, we chose 9-μm PVDF-TrFE material as the second matching layer, the thickness option available from the manufacturer that most closely approximated the optimal design value.

The 3-D model in OnScale Lab was designed with a 9-μm PVDF-TrFE layer and variable glue layer thickness, with the silver volume concentration fixed at 21.5% for the chosen conductive glue. Fig. 7(a) shows the results from the parameterization study for which only the silver-epoxy glue thickness was varied from 1 to 40 μm in 100 nm steps. There is a continuous trade-off between sensitivity and bandwidth while increasing the thickness, reaching their maxima for low thickness values below 15 μm. Based on these results, we chose 7-μm as a compromise to increase sensitivity while keeping the FBW close to the original value, in contrast with the initial 8.3-μm optimal value from the 1-D model, where a different silver volume fraction was used. Fig. 7(b) and (c) shows the echo response for the bare and the final acoustic stack, reflecting the final stack improvement of 3.54 dB in sensitivity.

B. Stack Characterization

We prepared and populated six PCBs: 3 of them only holding the piezocomposite and three additional ones with the whole acoustic stack. A summary of the US characterization results for all the stacks is presented in Table IV, while the individual results for a complete stack are illustrated in Fig. 8(a)–(d). The margins of error for the lateral and axial resolution values are determined by the *XYZ* stage step (5 μm) and the sampling frequency of the acquisition card (400 MHz), respectively. Every experiment was repeated and averaged 8 times to reduce errors due to vibrations of the setup during scanning.

Fig. 8(e) and (f) illustrates the results from the PA experiment with the complete acoustic stack. According to the PA signal captured by the hydrophone, its frequency content spans at least the whole available bandwidth (1–35 MHz). The PA signals were captured simultaneously by the LF receiver and

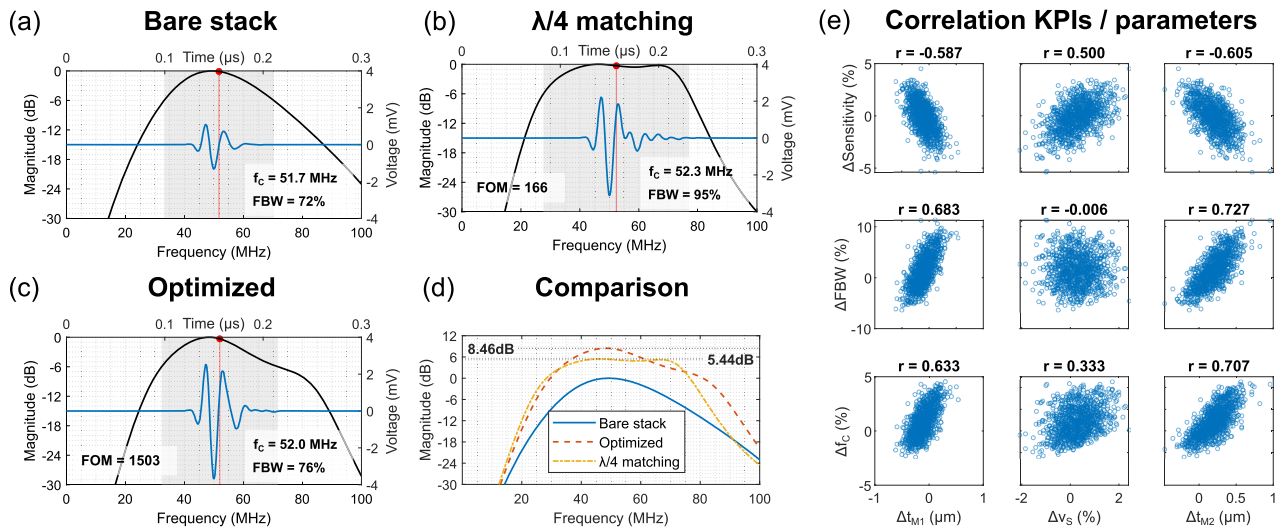

Fig. 6. Acoustic stack KLM simulation results. (a)–(c) Echo time and frequency responses of (a) bare stack, and the stack with (b) $\lambda/4$ and (c) optimized matching layers. FOM values are shown for the stacks with matching layers. (d) Comparison of the frequency responses with magnitude normalized on the value of the stack with no matching layers. The maximum value for $\lambda/4$ and optimized matching layers stack response is indicated with a dotted horizontal line. (e) Correlation between variables for the stack and KPIs. Each plot is labeled with the Pearson's correlation coefficient (r), where a value closer to ± 1 signifies a high linear relation. FBW: -6 dB fractional bandwidth, f_C: center frequency, FOM: figure of merit, t_{M1}: first matching layer thickness, v_S: first matching layer silver volume fraction, t_{M2}: second matching layer thickness.

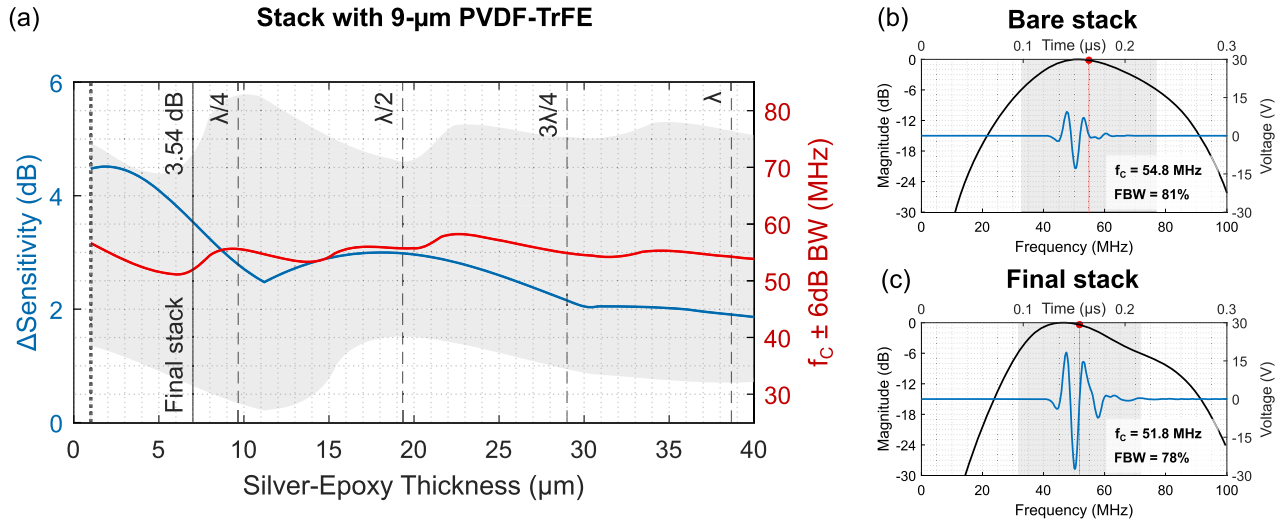

Fig. 7. Acoustic stack OnScale Lab simulation results. (a) First matching layer thickness sweep from 1 to 40 μm. Δ Sensitivity (blue) is measured as the ratio between the peak value of the frequency response respect to the bare stack result. Center frequency is presented in red and -6 dB bandwidth as the gray area around it. The final stack value is presented as a vertical line at 7 μm. Different multiples of $\lambda/4$ thickness are presented as vertical dashed lines. (b) and (c) Echo time and frequency responses of (b) bare stack and (c) final stack with a 7-μm first matching layer. FBW: -6 dB fractional bandwidth, f_C: center frequency.

TABLE IV
SUMMARY OF FABRICATED STACKS PERFORMANCE

#	Stack	V_{PP} (mV)	A_{PEAK} (dB)	FBW (%)	f_C (MHz)	PL (ns)	AR ($\pm$ 3.75 μm)	LR ($\pm$ 5 μm)
1	Bare	288	0.00	55	60.3	47	26.25	205
2	Bare	309	0.56	54	61.2	48	26.25	215
3	Bare	284	0.45	52	59.7	58	26.25	220
4	Complete	334	0.36	84	51.5	33	26.25	190
5	Complete	300	0.36	74	51.9	66	22.50	215
6	Complete	400	1.39	85	52.4	36	22.50	210

V_{PP}: peak-to-peak voltage, A_{PEAK}: maximum value of frequency response, normalized to stack #1 value, FBW: -6 dB fractional bandwidth, f_C: center frequency, PL: -20 dB pulse length, AR: axial resolution, LR: lateral resolution.

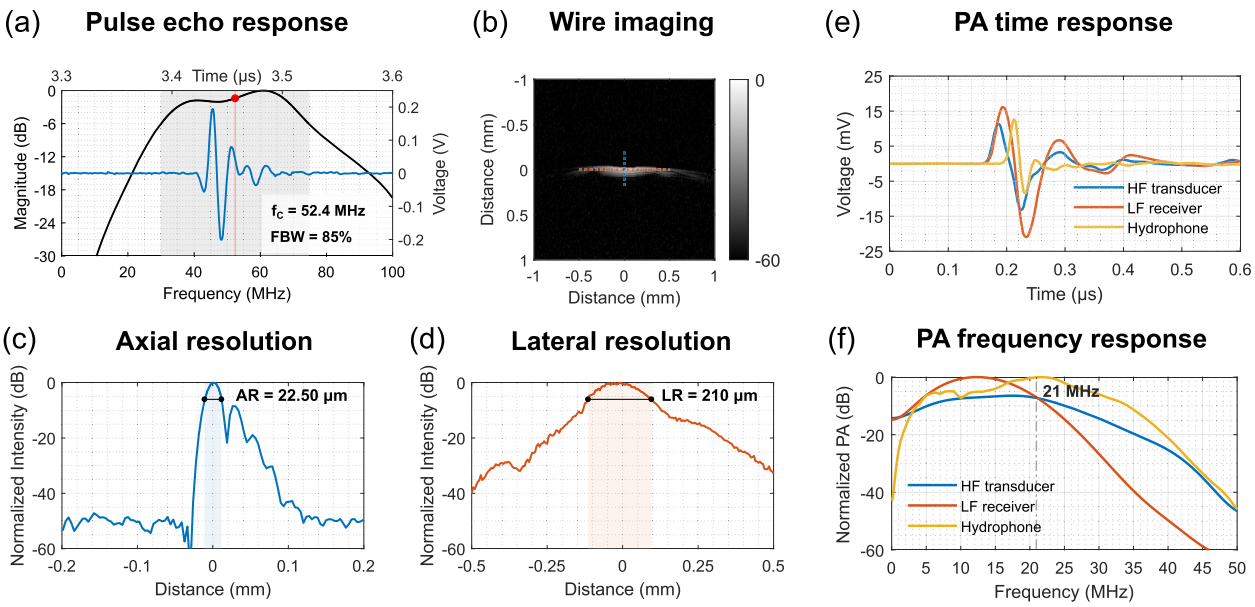

Fig. 8. (a)–(d) Stack #6 US and (e) and (f) PA characterization results. (a) Time and frequency response of the pulse-echo experiment targeting a silver-coated mirror. (b) US imaging of a 15-μm wire at the natural focus of the transducer and 60 dB dynamic range. (c) Axial and (d) lateral profiles of the wire and resolution measured as the -6 dB area around their maxima. (e) Time and (f) frequency response of the first and second PA experiment targeting black tape, respectively. Frequency responses are normalized to their maximum value, except for the HF transducer, which is normalized respect to the LF receiver response. FBW: -6 dB fractional bandwidth, f_C: center frequency.

HF transducer. Fig. 8(e) shows the time signals from the LF and HF layers, along with the hydrophone signal, where the LF receiver intensity is higher than that of the HF transducer. For a first experiment where LF receiver intensity is higher than that of the HF transducer. Fig. 8(f) shows the frequency normalized response of the signals, received by the two transducers, jointly normalized to the hydrophone trace and relative to the LF receiver response. The signal captured by the LF receiver remains higher until 21 MHz, above which the HF transducer becomes more sensitive. Time and frequency plots in Fig. 8(e) and (f) were acquired in different experiments, which differed in alignment and amplification.

IV. Discussion

In this study, we have designed, fabricated, and characterized a dual-transducer acoustic stack incorporating a 1–3 PMN-PT/epoxy piezocomposite and a PVDF-TrFE-based transducer for high-resolution pulse-echo and broadband PA reception. Our results demonstrate the potential of such a stack for multifrequency intravascular imaging without increasing the catheter's tip length or diameter beyond conventional dimensions. After comparing the US performance between single- and dual-transducer configurations using 1-D and 3-D models, we have shown that the fabricated stack results align with the simulation predictions regarding sensitivity and bandwidth improvement.

Moreover, the experiments confirm the stack's suitability as a combined PA receiver and pulse-echo transducer. In PA receive mode, the LF element provided a signal that is larger below 21 MHz than this particular HF element, which also demonstrated considerable receive sensitivity at low frequencies. Signals from atherosclerotic plaque had relatively lower HF content than the black-tape target used here [6], and the benefit of the LF receiver in representing the total signal would be even more significant than it is here. Further stacks and phantoms would need to be manufactured to thoroughly characterize the stack as a combined pulse-echo and PA imaging device in a catheter configuration.

The variation in performance between different stacks highlights a fabrication challenge: achieving a uniform silver-epoxy layer thickness. The current fabrication process likely contributed to this discrepancy due to a nonuniform glue layer thickness, as the small stack elements are manually assembled with no subsequent verification of the actual thickness or alignment. Additionally, the size of silver particles within the composite can restrict the minimum glue layer thickness. These issues could be addressed by choice of glue with a controlled maximum particle size and by introducing more advanced manufacturing techniques like pick-and-place machines. The presented configuration of the stack working along the ASIC requires using two independent acquisition channels on the system side. Further development of the ASIC can potentially enable a single-channel acquisition design.

V. Conclusion

We have developed and validated a dual-transducer stack for combined IVUS/PA imaging. The stack design we propose demonstrates that it is possible to achieve PA acquisition and US imaging using a compact transducer arrangement without sacrificing pulse-echo performance. Future work will focus on improving the fabrication process and fine-tuning the acoustic stack parameters. This work can be the base for incorporating this technology into a catheter prototype, enhancing IVUS/PA imaging to become a viable tool for intravascular diagnostic imaging.

Conflict of Interest

Gijs van Soest is a scientific advisor of, and has a financial interest in, Kaminari Medical B.V., Rotterdam,

The Netherlands, a company developing IVPA technology. Antonius F. W. van der Steen is a strategic advisor of, and has a financial interest in, Kaminari Medical B.V. Verya Daeichin is employed by and has a financial interest in Kaminari Medical B.V.

Acknowledgment

The authors would like to thank Emile Noothout, TU Delft, Delft, The Netherlands, for assistance with application-specific integrated circuits (ASICs), and the stack fabrication, and Stein Beekenkamp, Erasmus MC University Medical Center, Rotterdam, The Netherlands, for fabrication support. They would also like to thank Jian Tian and Cedric Goueffon, CTS Corporation, Lisle, IL, USA, for their assistance on how to use the piezocomposite transducers.

References

[1] S. Dattani, V. Samborska, H. Ritchie, and M. Roser. (2023). *Cardiovascular Diseases*. [Online]. Available: https://ourworldindata.org/cardiovascular-diseases

[2] P. Libby, "The changing landscape of atherosclerosis," *Nature*, vol. 592, no. 7855, pp. 524–533, Apr. 2021, doi: 10.1038/s41586-021-03392-8.

[3] C. V. Bourantas et al., "Hybrid intravascular imaging: Recent advances, technical considerations, and current applications in the study of plaque pathophysiology," *Eur. Heart J.*, vol. 38, no. 6, pp. 400–412, Feb. 2017, doi: 10.1093/eurheartj/ehw097.

[4] T. Zhao, A. E. Desjardins, S. Ourselin, T. Vercauteren, and W. Xia, "Minimally invasive photoacoustic imaging: Current status and future perspectives," *Photoacoustics*, vol. 16, Dec. 2019, Art. no. 100146, doi: 10.1016/j.pacs.2019.100146.

[5] G. Xu, J. B. Fowlkes, C. Tao, X. Liu, and X. Wang, "Photoacoustic spectrum analysis for microstructure characterization in biological tissue: Analytical model," *Ultrasound Med. Biol.*, vol. 41, no. 5, pp. 1473–1480, May 2015, doi: 10.1016/j.ultrasmedbio.2015.01.010.

[6] V. Daeichin, M. Wu, N. De Jong, A. F. W. van der Steen, and G. van Soest, "Frequency analysis of the photoacoustic signal generated by coronary atherosclerotic plaque," *Ultrasound Med. Biol.*, vol. 42, no. 8, pp. 2017–2025, Aug. 2016, doi: 10.1016/j.ultrasmedbio.2016.03.015.

[7] A. B. Karpiouk, B. Wang, and S. Y. Emelianov, "Development of a catheter for combined intravascular ultrasound and photoacoustic imaging," *Rev. Sci. Instrum.*, vol. 81, no. 1, Jan. 2010, Art. no. 014901, doi: 10.1063/1.3274197.

[8] K. Jansen, A. F. W. van der Steen, H. M. M. van Beusekom, J. W. Oosterhuis, and G. van Soest, "Intravascular photoacoustic imaging of human coronary atherosclerosis," *Opt. Lett.*, vol. 36, no. 5, p. 597, Mar. 2011, doi: 10.1364/ol.36.000597.

[9] M. Abran, G. Cloutier, M. R. Cardinal, B. Chayer, J.-C. Tardif, and F. Lesage, "Development of a photoacoustic, ultrasound and fluorescence imaging catheter for the study of atherosclerotic plaque," *IEEE Trans. Biomed. Circuits Syst.*, vol. 8, no. 5, pp. 696–703, Oct. 2014, doi: 10.1109/TBCAS.2014.2360560.

[10] X. Bai et al., "Intravascular optical-resolution photoacoustic tomography with a 1.1 mm diameter catheter," *PLoS One*, vol. 9, no. 3, Mar. 2014, Art. no. e92463, doi: 10.1371/journal.pone.0092463.

[11] Y. Li et al., "High-speed intravascular spectroscopic photoacoustic imaging at 1000 A-lines per second with a 0.9-mm diameter catheter," *J. Biomed. Opt.*, vol. 20, no. 6, p. 10, Jun. 2015, doi: 10.1117/1.jbo.20.6.065006.

[12] J. Hui et al., "Real-time intravascular photoacoustic-ultrasound imaging of lipid-laden plaque in human coronary artery at 16 frames per second," *Sci. Rep.*, vol. 7, no. 1, p. 1417, May 2017, doi: 10.1038/s41598-017-01649-9.

[13] D. VanderLaan, A. B. Karpiouk, D. Yeager, and S. Emelianov, "Real-time intravascular ultrasound and photoacoustic imaging," *IEEE Trans. Ultrason., Ferroelectr., Freq. Control*, vol. 64, no. 1, pp. 141–149, Jan. 2017, doi: 10.1109/TUFFC.2016.2640952.

[14] Y. Li et al., "PMN-PT/Epoxy 1–3 composite based ultrasonic transducer for dual-modality photoacoustic and ultrasound endoscopy," *Photoacoustics*, vol. 15, Sep. 2019, Art. no. 100138, doi: 10.1016/j.pacs.2019.100138.

[15] P. Lei, X. Wen, L. Wang, P. Zhang, and S. Yang, "Ultrafine intravascular photoacoustic endoscope with a 07 mm diameter probe," *Opt. Lett.*, vol. 44, no. 22, p. 5406, Nov. 2019, doi: 10.1364/ol.44.005406.

[16] W. Wei, X. Li, Q. Zhou, K. K. Shung, and Z. Chen, "Integrated ultrasound and photoacoustic probe for co-registered intravascular imaging," *J. Biomed. Opt.*, vol. 16, no. 10, Oct. 2011, Art. no. 106001, doi: 10.1117/1.3631798.

[17] J. Hui et al., "High-speed intravascular photoacoustic imaging at 17 μm with a KTP-based OPO," *Biomed. Opt. Exp.*, vol. 6, no. 11, p. 4557, Nov. 2015, doi: 10.1364/boe.6.004557.

[18] R. Lin et al., "Miniature intravascular photoacoustic endoscopy with coaxial excitation and detection," *J. Biophotonics*, vol. 16, no. 4, Apr. 2023, Art. no. e202200269, doi: 10.1002/jbio.202200269.

[19] B.-Y. Hsieh, S.-L. Chen, T. Ling, L. J. Guo, and P.-C. Li, "Integrated intravascular ultrasound and photoacoustic imaging scan head," *Opt. Lett.*, vol. 35, no. 17, p. 2892, Sep. 2010, doi: 10.1364/ol.35.002892.

[20] B. Dong, S. Chen, Z. Zhang, C. Sun, and H. F. Zhang, "Photoacoustic probe using a microring resonator ultrasonic sensor for endoscopic applications," *Opt. Lett.*, vol. 39, no. 15, p. 4372, Aug. 2014, doi: 10.1364/ol.39.004372.

[21] E. Z. Zhang and P. C. Beard, "A miniature all-optical photoacoustic imaging probe," in *Photons Plus Ultrasound: Imaging and Sensing*. Bellingham, WA, USA: SPIE, 2011, doi: 10.1117/12.874883.

[22] S. J. Mathews et al., "All-optical dual photoacoustic and optical coherence tomography intravascular probe," *Photoacoustics*, vol. 11, pp. 65–70, Sep. 2018, doi: 10.1016/j.pacs.2018.07.002.

[23] X. Ji, K. Xiong, S. Yang, and D. Xing, "Intravascular confocal photoacoustic endoscope with dual-element ultrasonic transducer," *Opt. Exp.*, vol. 23, no. 7, p. 9130, Apr. 2015, doi: 10.1364/oe.23.009130.

[24] Y. Cao, M. Alloosh, M. Sturek, and J. Cheng, "Highly sensitive lipid detection and localization in atherosclerotic plaque with a dual-frequency intravascular photoacoustic/ultrasound catheter," *Translational Biophotonics*, vol. 2, no. 3, pp. 1–26, Aug. 2020, doi: 10.1002/tbio.202000004.

[25] V. Daeichin et al., "A broadband polyvinylidene difluoride-based hydrophone with integrated readout circuit for intravascular photoacoustic imaging," *Ultrasound Med. Biol.*, vol. 42, no. 5, pp. 1239–1243, May 2016, doi: 10.1016/j.ultrasmedbio.2015.12.016.

[26] W. Qiu, Y. Chen, C.-M. Wong, B. Liu, J. Dai, and H. Zheng, "A novel dual-frequency imaging method for intravascular ultrasound applications," *Ultrasonics*, vol. 57, pp. 31–35, Mar. 2015, doi: 10.1016/j.ultras.2014.10.011.

[27] S. Yoon et al., "Dual-element needle transducer for intravascular ultrasound imaging," *J. Med. Imag.*, vol. 2, no. 2, Apr. 2015, Art. no. 027001, doi: 10.1117/1.jmi.2.2.027001.

[28] J. Hong et al., "A dual-mode imaging catheter for intravascular ultrasound application," *IEEE Trans. Med. Imag.*, vol. 38, no. 3, pp. 657–663, Mar. 2019, doi: 10.1109/TMI.2018.2869942.

[29] J. Lee and J. H. Chang, "Dual-element intravascular ultrasound transducer for tissue harmonic imaging and frequency compounding: Development and imaging performance assessment," *IEEE Trans. Biomed. Eng.*, vol. 66, no. 11, pp. 3146–3155, Nov. 2019, doi: 10.1109/TBME.2019.2901005.

[30] Z. Jiang, R. J. Dickinson, T. L. Hall, and J. J. Choi, "A PZT–PVDF stacked transducer for short-pulse ultrasound therapy and monitoring," *IEEE Trans. Ultrason., Ferroelectr., Freq. Control*, vol. 68, no. 6, pp. 2164–2171, Jun. 2021, doi: 10.1109/TUFFC.2021.3059715.

[31] H. Wu et al., "Miniaturized stacked transducer for intravascular sonothrombolysis with internal-illumination photoacoustic imaging guidance and clot characterization," *IEEE Trans. Biomed. Eng.*, vol. 70, no. 8, pp. 2279–2288, Aug. 2023, doi: 10.1109/TBME.2023.3240725.

[32] J. Ma, K. H. Martin, P. A. Dayton, and X. Jiang, "A preliminary engineering design of intravascular dual-frequency transducers for contrast-enhanced acoustic angiography and molecular imaging," *IEEE Trans. Ultrason., Ferroelectr., Freq., Control*, vol. 61, no. 5, pp. 870–880, May 2014, doi: 10.1109/TUFFC.2014.2977.

[33] X. Li, W. Wei, Q. Zhou, K. K. Shung, and Z. Chen, "Intravascular photoacoustic imaging at 35 and 80 MHz," *J. Biomed. Opt.*, vol. 17, no. 10, Oct. 2012, Art. no. 1060051, doi: 10.1117/1.jbo.17.10.106005.

[34] X. Ma and W. Cao, "Single-crystal high-frequency intravascular ultrasound transducer with 40-μ m axial resolution," *IEEE Trans. Ultrason., Ferroelectr., Freq. Control*, vol. 67, no. 4, pp. 810–816, Apr. 2020, doi: 10.1109/TUFFC.2019.2956603.

[35] W. A. Smith and B. A. Auld, "Modeling 1–3 composite piezoelectrics: Thickness-mode oscillations," *IEEE Trans. Ultrason., Ferroelectr., Freq. Control*, vol. 38, no. 1, pp. 40–47, Jan. 1991, doi: 10.1109/58.67833.

[36] C. S. Desilets, J. D. Fraser, and G. S. Kino, "The design of efficient broad-band piezoelectric transducers," *IEEE Trans. Sonics Ultrason.*, vols. SU-25, no. 3, pp. 115–125, May 1978, doi: 10.1063/1.91949.
[37] A. J. Devaney and H. Levine, "Effective elastic parameters of random composites," *Appl. Phys. Lett.*, vol. 37, no. 4, pp. 377–379, Aug. 1980, doi: 10.1063/1.91949.
[38] R. Krimholtz, D. A. Leedom, and G. L. Matthaei, "New equivalent circuits for elementary piezoelectric transducers," *Electron. Lett.*, vol. 6, no. 13, p. 398, 1970, doi: 10.1049/el:19700280.

Antonio López-Marín (Member, IEEE) received the B.Sc. and M.Sc. degrees in telecommunication engineering from the University of Seville, Seville, Spain, in 2015, and the M.Sc. degree in biomedical engineering from the University of Barcelona, Barcelona, Spain, in 2019. He is currently pursuing the Ph.D. degree with the Department of Biomedical Engineering, Erasmus Medical Center, Rotterdam, The Netherlands.

After graduating in 2015, he was with the Research Center for Biomedical Engineering, Barcelona, as an Electronics Engineer, developing wearable systems for activity tracking in health and sports. His research interests include medical device development involving signal and image processing, electronics design, and control systems using ultrasonics, optics, and bioimpedance.

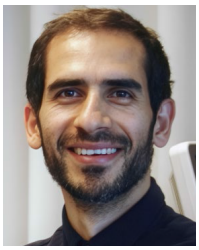

Verya Daeichin (Member, IEEE) received the Ph.D. degree in biomedical engineering from the Erasmus Medical Center, Rotterdam, The Netherlands, in 2015.

Following this, he pursued postdoctoral research with Erasmus MC University Medical Center, TU Delft, Delft, The Netherlands, and the University of Colorado Boulder, Boulder, CO, USA, contributing to various interdisciplinary projects, from 2015 to 2021. In 2021, he joined Kaminari Medical B.V., Rotterdam, a spin-off from the Erasmus MC University Medical Center, where he is currently the Chief Technology Officer. As one of the inventors, he is leading the development of an innovative intravascular imaging catheter that integrates both ultrasound and photoacoustic imaging technologies.

Andres Hunt received the M.Sc. degree in applied physics from the University of Tartu, Tartu, Estonia, in 2009, and the Ph.D. degree in computer and systems engineering from Tallinn University of Technology, Tallinn, Estonia, in 2017.

After his Ph.D. studies, he joined Delft University of Technology, Delft, The Netherlands, as a Postdoctoral Researcher with the Mechatronic System Design Group, Department of Precision and Microsystems Engineering. Since 2020, he continued as an Assistant Professor with the Micro and Nano Engineering Group, Department of Precision and Microsystems Engineering. His research investigates embedding actuation, sensing, and smart functionalities into the otherwise passive materials, structures, mechanisms, and devices. It entails developing: 1) technologies to create high-performance and versatile actuators; 2) multimaterial additive manufacturing methods to realize embedded functionalities; 3) materials that function as mechatronic systems or subsystems; and 4) their utilization.

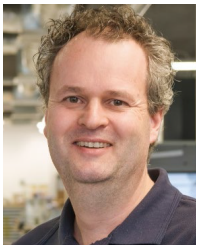

Geert Springeling received the B.Eng. degree in mechanical engineering from Hogeschool Utrecht, Amersfoort, The Netherlands, in 2010.

Since 2005, he has been with the Department EMI, Erasmus MC University Medical Center, Rotterdam, The Netherlands. He worked on intravascular ultrasound, intravascular photoacoustic, and OCT catheter development. His research interests include precision engineering, micro mechanics, and (fiber)-optics.

Robert Beurskens received the B.Sc. degree in electrical engineering from Fontys Hogeschool Venlo, Venlo, The Netherlands, in 1997.

After pursuing his degree, he started working at Hauzer Techno Coating, Venlo, as an Electrical Engineer, involved in industrial scale physical vapor deposition (PVD) equipment. In 1999, he started to work at the Prins Maurits Laboratorium, Rijswijk, The Netherlands, a branch of Dutch Organization for Applied Physics, TNO, The Hague, The Netherlands. Since 2007, he has been with the Department of Biomedical Engineering, Erasmus MC University Medical Center, Rotterdam, The Netherlands, as an Electronic Designer and an Instrumentation Technician. His main interest was the design, construction, and operation of high voltage pulsed power systems for all kinds of civil and defense applications varying from food stuff sterilization, atmospheric plasma's to electric reactive armor, and counter measures. His research interests include mechatronics and analog high-frequency electronics for ultrasound applications.

Antonius F. W. van der Steen (Fellow, IEEE) received the M.Sc. degree in applied physics from Technical University Delft, Delft, The Netherlands, in 1989, and the Ph.D. degree in medical science from Catholic University Nijmegen, Nijmegen, The Netherlands, in 1994.

He is currently the Head of the Biomedical Engineering, Thorax Center, Erasmus MC University Medical Center, Rotterdam, The Netherlands. He is an Expert in ultrasound, cardiovascular imaging, and cardiovascular biomechanics. He has a career at the crossroads of engineering, health care, and industry. He was the Co-PI of ParisK, one of the large CTMM projects (16 million €). His international profile is high, with more than 200 invited lectures all over the world, and a Guest Professorship/Guest Researcher in Canada, Japan, and China.

Dr. van der Steen is a fellow of European Society of Cardiology. He is a member of The Netherlands Academy of Technology (AcTI) and a Board Member of the Royal Netherlands Academy of Sciences (KNAW). He was a recipient of the Simon Stevin Master Award and the NWO PIONEER Award in Technical Sciences. He has experience in running large consortia as the Co-Founder and the former Chair of the Medical Delta, which comprises over 280 scientists working on technical solutions for sustainable health.

Gijs van Soest received the M.Sc. degree from the University of Groningen, Groningen, The Netherlands, in 1997, and the Ph.D. degree from the University of Amsterdam, Amsterdam, The Netherlands, in 2001.

He is currently a Professor with the Department of Cardiology, Erasmus MC University Medical Center, Rotterdam, The Netherlands, and leads the research group, a part of the Biomedical Engineering Laboratory, that specializes in the development of catheter-based and endoscopic imaging technologies based on light, ultrasound, and combinations thereof. As a Medical Delta Professor with the Department of Precision and Microsystems Engineering, Faculty of Mechanical Engineering, Delft University of Technology, Delft, The Netherlands, he investigates advanced medical instrument technologies, design, and manufacturing methods. Being trained as an Experimental Physicist, he worked on atmospheric remote sensing before dedicating himself to interventional imaging in cardiology. He is the Founder of Kaminari Medical B.V., Rotterdam, a company developing intravascular photoacoustic imaging. He is also the Scientific Director and the Founder of the Image Guidance in Percutaneous Coronary Interventions (iPCI).